



# CHORUS

This is the accepted manuscript made available via CHORUS. The article has been published as:

## Energy scales of the doped Anderson lattice model

Hanhim Kang, Kristjan Haule, Gabriel Kotliar, Piers Coleman, and Ji-Hoon Shim

Phys. Rev. B **99**, 165115 — Published 12 April 2019

DOI: [10.1103/PhysRevB.99.165115](https://doi.org/10.1103/PhysRevB.99.165115)

# Energy Scales of the Doped Anderson Lattice Model

Hanhim Kang

*Department of Chemistry, Pohang University of Science and Technology, Pohang 790-784, Korea*

Kristjan Haule, Gabriel Kotliar, and Piers Coleman

*Department of Physics and Astronomy, Rutgers University, NJ, USA*

Ji-Hoon Shim\*

*Department of Chemistry, Pohang University of Science and Technology, Pohang 790-784, Korea and*

*Department of Physics, Pohang University of Science and Technology, Pohang 790-784, Korea*

(Dated: March 18, 2019)

This paper explores the energy scales of the doped Anderson lattice model using dynamical mean-field theory (DMFT), using a continuous-time Quantum Monte Carlo (CTQMC) impurity solver. We show that the low temperature properties of the lattice can not be scaled using the single ion local Kondo temperature  $T_K$  but instead are governed by a doping-dependent coherence temperature  $T^*$  which can be used to scale the temperature dependence of the spectral function, transport properties, and entropy. At half filling  $T^*$  closely approximates the single ion  $T_K$ , but as the filling  $n_c$  is reduced to zero,  $T^*$  also vanishes. The coherence temperature  $T^*$  is shown to play a role of effective impurity Kondo temperature in the lattice model, and physical observables show significant evolution at  $T^*$ . In the DMFT framework, we showed that the hybridization strength of the effective impurity model is qualitatively affected by the doping level, and determines  $T^*$  in the lattice model.

The Kondo effect was first observed as a resistivity minimum in dilute magnetic alloys<sup>1</sup>. Jun Kondo accounted for the resistivity minimum as a consequence of an antiferromagnetic super-exchange between the magnetic impurity and conduction electrons<sup>2</sup>. This antiferromagnetic coupling was later revealed to be a relevant coupling, renormalizing to strong coupling at a characteristic energy scale called the Kondo temperature<sup>3-6</sup>. Based on a strong-coupling expansion, Nozières showed that the ground state of a magnetically screened Kondo impurity is described by a local Fermi liquid<sup>7</sup>. After that, a slave-particle mean-field theory showed that Kondo physics can be understood as the residue of a symmetry-breaking transition that occurs in the large  $N$  limit of the spin degeneracy, in which the Kondo temperature plays the role of a critical temperature for the phase transition<sup>8,9</sup>.

In a large class of  $f$ -electron intermetallic materials called “heavy electron” compounds, such as the family of 115 compounds,  $\text{Ce}M\text{In}_5$  ( $M=\text{Co,Rh,Ir}$ ), the localized  $f$  electrons form a periodic lattice of magnetic moments whose low energy physics is described by a Kondo lattice model<sup>10</sup>. A generic phase diagram of the Kondo lattice was proposed by Doniach<sup>11</sup>, who argued that if the Kondo coupling is weak the magnetic Ruderman-Kittel-Kasuya-Yosida (RKKY) interaction overcomes the formation of Kondo singlets, giving rise to an ordered magnetic ground-state<sup>10,12,13</sup>. This state has a small Fermi surface because only the conduction electrons contribute to the charge transport. However, if the Kondo coupling is strong, it gives rise to a paramagnetic ground state which resembles the Nozières Fermi liquid state of the Kondo impurity model. Such “heavy fermi liquids”

(HFL) display carrier effective masses up to  $\sim 10^3$  times larger than in conventional metals. In the HFL state, the localized moments bind to electrons, forming composite  $f$ -quasiparticles which hybridize with the conduction sea, giving rise to an enlarged Fermi surface of heavy quasiparticles.

One of the long-standing questions concerns how the HFL phase evolves upon raising the temperature, and in particular, whether additional scales, beyond the single-ion Kondo temperature, are required to describe the gradual loss of coherence in the HFL<sup>14-18</sup>. Theoretically, the slave-boson approach showed that an additional low energy Fermi-liquid energy scale ( $T_{FL}$ ) develops in HFL<sup>19</sup>. Later numerical studies using the dynamical mean-field theory (DMFT) confirmed that this Fermi-liquid energy scale exists, identifying it as the temperature at which resistivity develops a maximum<sup>20</sup>. However, there is still no final consensus between these different studies on the precise relationship between the coherence temperature scale and the evolution of the large Fermi surface<sup>19-22</sup>. These considerations motivate an integrated study of thermodynamic, transport, and spectroscopic properties of the Kondo lattice model, with the goal of connecting experimental, analytic, and numerical studies.

In this letter, we report on a detailed study of Anderson lattice model in the Kondo lattice regime using DMFT<sup>23-26</sup>, with a continuous-time Quantum Monte Carlo (CTQMC) impurity solver<sup>27</sup>. The study varied the hybridization strength, temperature, and the doping level to cover wide range of the phase diagram and investigate the scaling properties. Maximum-entropy methods were

used to analytically continue from imaginary to real time to obtain dynamical spectral functions<sup>28,29</sup>.

The single-orbital Anderson lattice model is written as

$$H = \sum_{i\sigma} \epsilon_f f_{i\sigma}^\dagger f_{i\sigma} + U \sum_i n_{i\uparrow}^f n_{i\downarrow}^f - t \sum_{\langle ij \rangle \sigma} (c_{i\sigma}^\dagger c_{j\sigma} + H.c.) + V \sum_{i\sigma} (c_{i\sigma}^\dagger f_{i\sigma} + H.c.) - \mu \sum_{i\sigma} (n_{i\sigma}^f + n_{i\sigma}^c) \quad (1)$$

where  $f_{i\sigma}^\dagger$  ( $f_{i\sigma}$ ) is a creation (annihilation) operator of the  $f$  electron with spin  $\sigma$  at site  $i$ ,  $c_{i\sigma}^\dagger$  ( $c_{i\sigma}$ ) is a creation (annihilation) operator of the conduction electron with spin  $\sigma$  at site  $i$ , and  $n_{i\sigma}^\alpha = \alpha_{i\sigma}^\dagger \alpha_{i\sigma}$  ( $\alpha = f, c$ ).

For convenience, all energy scales are written in units of  $D$ , the half bandwidth of the conduction band, and the Boltzmann constant  $k_B$  is set to unity. We considered a two-dimensional square lattice with half bandwidth  $D = 4t$ . To achieve the Kondo lattice regime, we place the  $f$ -level at the bottom of the band, choosing  $\epsilon_f = -1.0$  and set  $U = 2.0$ , so that the energy of the doubly occupied state  $\epsilon_f + U = 1.0$  lies at the top of band. The hybridization  $V$ , chemical potential  $\mu$ , and inverse temperature  $\beta$  were varied from 0.18 to 0.54,  $-0.8$  to  $0.8$ , and  $80.00$  to  $200.00$ , respectively.

Figure 1 (a) shows the local spin susceptibility  $\chi_{loc}(\omega = 0)$  for  $\mu = -0.8$ , for a variety of hybridization values  $V$ , scaled by the single-impurity Kondo temperature  $T_K$  evaluated with the same parameters, defined by

$$T_K = \sqrt{2J_K \rho} \exp \left[ -\frac{1}{2J_K \rho} \right] \quad (2)$$

where  $\rho$  is the density of states per spin of the conduction band at the Fermi level and  $J_K = (|\epsilon_f - \mu|^{-1} + |\epsilon_f - \mu + U|^{-1})V^2$  is the Kondo exchange<sup>30</sup>. Because the undoped model ( $\mu = 0.0$ ) is particle-hole symmetric, electron and hole doped cases behave identically<sup>31</sup>. The scaling collapse of the susceptibility curves at high temperatures  $\chi_{loc}(T) \sim \frac{1}{T} f(T/T_K)$  shows that the high temperature physics of the Anderson lattice model is scaled by the single-ion Kondo temperature, regardless of the doping level<sup>31</sup>, implying that the high temperature physics at  $T > T_K$  is that of a single impurity model.

However the local susceptibility (Fig. 1 (a)) does not scale with the single-ion Kondo temperature at low temperatures. To scale the low- $T$  regime, we define a coherence temperature  $T^*$ , parameterized as

$$T^* = \sqrt{2J^{latt} \rho} \exp \left[ -\frac{1}{2J^{latt} \rho} \right] \quad (3)$$

where  $J^{latt} = jJ_K$  is an effective Kondo lattice exchange strength. The unique fitting parameter  $j$  is adjusted at each doping level to collapse the low temperature susceptibilities onto a single curve<sup>31</sup>. Figure 1 (b) shows that the low- $T$  susceptibilities are successfully scaled by  $T^*$

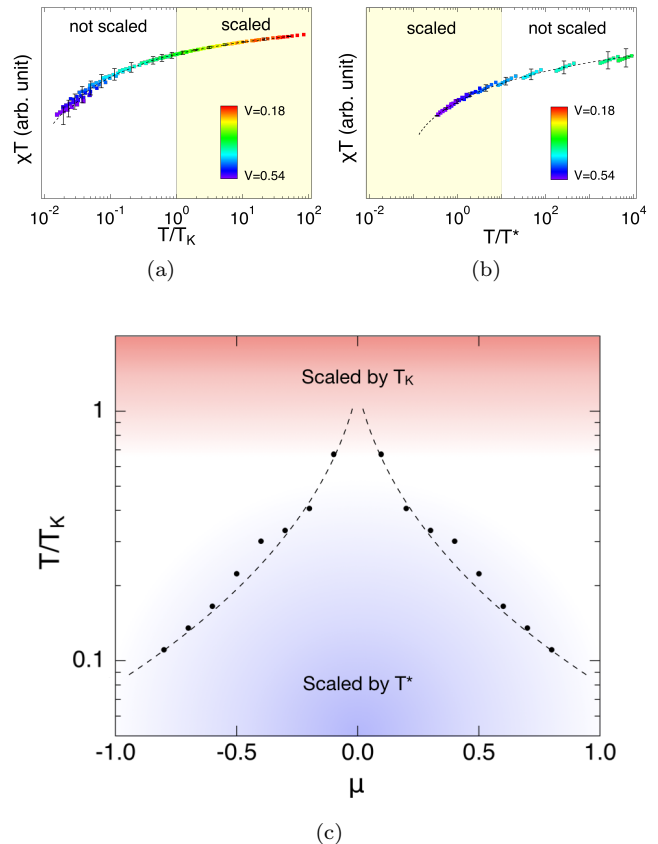


FIG. 1. Local static spin susceptibility of the Anderson lattice model scaled (a) by  $T_K$  and (b) by  $T^*$ , computed at chemical potential  $\mu = -0.8$ , for a range of hybridization between  $V = 0.18$  (red) and  $V = 0.54$  (purple). The dashed lines are the best-fit and the error bars show the mismatch between the best-fit line and actual data. (c) Schematic phase diagram showing the variation of  $T^*$  with chemical potential, and the regions where the data scales with  $T_K$  (red) and with  $T^*$  (blue). The dashed line is a guide to the eye.

with  $j = 0.3$ . The emergence of the temperature scale  $T^*$  indicates that the Kondo lattice model behaves differently in the fundamental level at low- $T$  regime.

Figure 1 (c) shows how  $T^*$  varies as the chemical potential is changed. When  $n_c$  is close to 0,  $T^*$  is suppressed towards zero while when  $n_c$  is close to half-filling,  $T^*$  tends towards the single-ion Kondo temperature  $T_K$ , a result that agrees with previous studies<sup>20</sup>.

Figure 2 (a) shows the calculated momentum- and energy-resolved total spectral function

$$A(\vec{k}, \omega) = \frac{1}{\pi} \text{Im} \left[ G_f(\vec{k}, \omega - i\delta) + G_c(\vec{k}, \omega - i\delta) \right] \quad (4)$$

at  $\mu = -0.5$  case. At high temperatures, only the coherent conduction band is observed near the Fermi level. Lowering the temperature, an incoherent  $f$ -electron spectrum develops at the Fermi level as a sign of Kondo singlet formation. It is notable that the spectral function starts to change far above the local Kondo temperature.

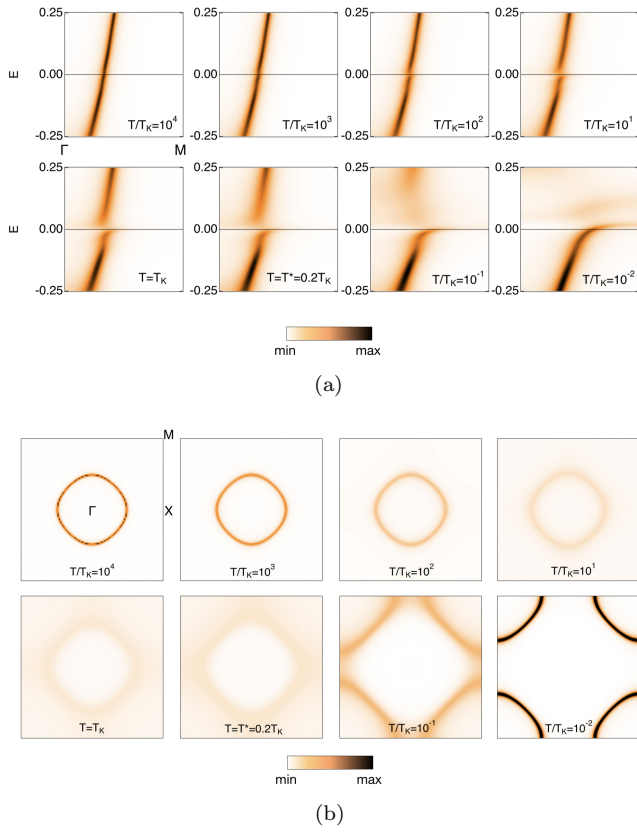


FIG. 2. Intensity plots showing the momentum and energy resolved conduction electron spectral function (a) as a function of momentum and (b) at fixed  $E = 0$ , showing the evolution of the Fermi surface with temperature, for  $\mu = -0.5$ .

It agrees well with recent ARPES measurement on the Ce-115 heavy fermion compound<sup>21,32</sup>. Crossing through  $T_K$ , the spectra near the Fermi level becomes incoherent, and the velocity of the ill-defined quasiparticles gets smaller as the  $f$ -electron develops near the Fermi energy. The spectrum is maximally incoherent at  $T = T^*$ , and the quasiparticle band only re-establishes its coherence below  $T^*$ .

Figure 2 (b) shows the evolution of the Fermi surface. Starting from a coherent small Fermi surface at high temperatures, it continuously evolves into an incoherent large Fermi surface, which sharpens well below the coherence temperature  $T^*$ . This continuous, but non-monotonic evolution of the Fermi surface gives a hint for nature of the non-Fermi liquid phase observed in the quantum critical region.

Figure 3 shows the area of the Fermi surface (a,b) and imaginary part of the  $T$ -matrix ( $T = V^2 G_f$ ) of the conduction band at the Fermi level (c,d) scaled by  $T_K$  and  $T^*$ . Even though  $T_K$  scales the high- $T$  behavior of both observables, there is no significant feature in both observables at  $T = T_K$ . For example, the small Fermi surface of the  $\mu = -0.8$  case does not evolve to the large Fermi surface phase until far below  $T = T_K$ . In contrast, both Fermi surface area and the  $f$ -electron DOS at the Fermi

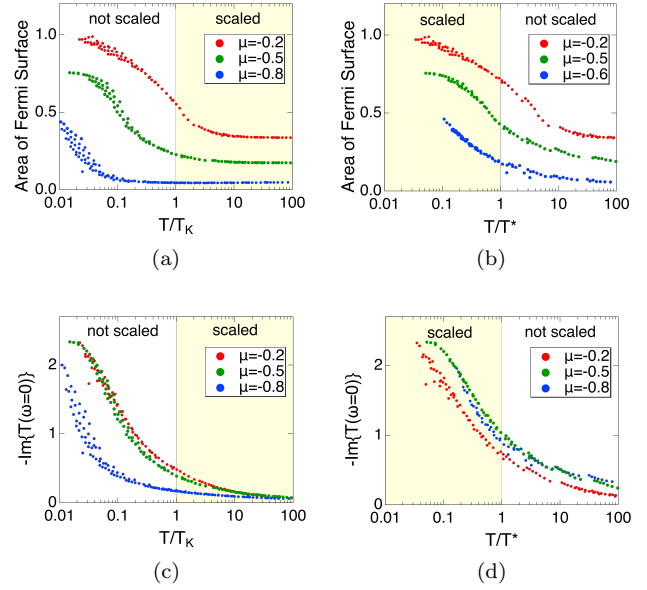


FIG. 3. Area of the Fermi surface (a,b) and imaginary part of the  $T$ -matrix of the conduction electrons at the Fermi level (c,d) scaled by  $T_K$  and  $T^*$ .

level evolve rapidly around  $T = T^*$ , regardless of the chemical potential.

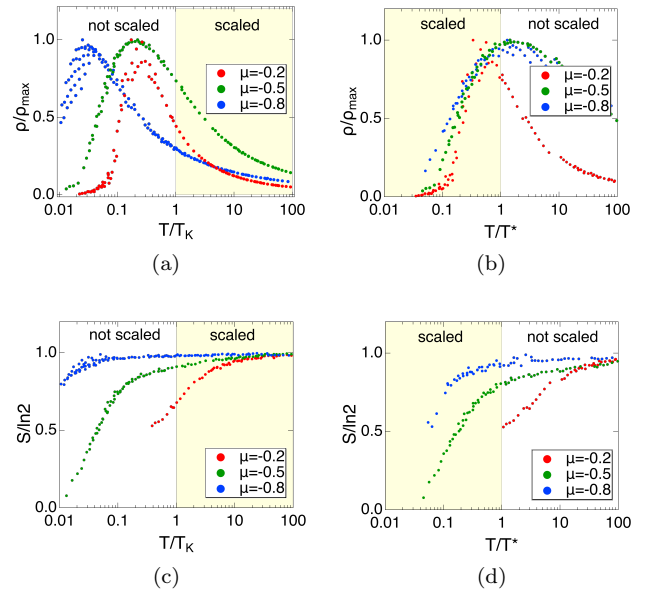


FIG. 4. Resistivity (a,b) and entropy (c,d) scaled by  $T_K$  and  $T^*$ .

The coherence temperature  $T^*$  also plays a significant role in the transport properties. Figure 4 shows the resistivity of  $\mu = -0.2, -0.5, -0.8$  cases. In the high- $T$  regime, the temperature dependence of the resistivity at different hybridization strengths can be scaled with the

local Kondo temperature  $T_K$  as Fig. 4 (a). As the temperature is reduced, the resistivity reaches a maximum and decreases forming a coherent HFL state. Figure 4 (b) shows that the low- $T$  resistivity is scaled by the coherence temperature  $T^*$ . In addition, the calculated resistivity develops its maximum value at temperatures  $T \sim T^*$  which lie below the single ion  $T_K$ . This suggests that experimentally observed resistivity maxima are related to  $T^*$  and can be used to estimate this quantity.

To investigate the screening of the local moments more directly, we also calculated the entropy of the impurity degree of freedom  $S$ . In Fig. 4 (c,d), the high temperature entropy approaches  $\ln 2$  per site, corresponding to the unscreened local moments of the  $f$ -electrons. It is remarkable that the entropy remains of order  $\sim \ln 2$  even at  $T < T_K$  in the heavily doped case ( $\mu = -0.8$ ) in Fig. 4 (c), indicating that the local moments are largely unscreened around  $T = T_K$ . Instead, as shown in Fig. 4 (d), the entropy starts to drop around  $T = T^*$  regardless of the doping level, although the amount of suppressed entropy depends on the doping level. The difference in the amount of suppressed entropy derives from the conduction electron occupancy  $n_c$ . Previous studies of the strong-coupling limit of the Kondo lattice model suggest that an entropy of order  $n_c \ln(2)$  is lost on passing through the Kondo temperature  $T_K$ <sup>33</sup>. However, our results show that the suppression of magnetic entropy  $S_M \sim n_c \ln(2)$  occurs at temperatures around  $T^*$ , rather than  $T_K$ .  $T^*$  thus sets the characteristic scale at which the moments become entangled with the conduction sea in the lattice.

In the DMFT framework, the Anderson lattice is treated as an effective impurity embedded in cavity with a self-consistently determined conduction electron bath. Figure 5 shows the self-consistent hybridization strength  $\Delta_0^{\text{latt.}} \equiv \text{Im}\Delta^{\text{eff.}}(z=0)$ , normalized by the bare hybridization strength of the model  $\Delta_0 \equiv \text{Im}\Delta(z=0)$ . In the lightly doped cases, ( $\mu = -0.2$ ) the effective hybridization function is enhanced at intermediate temperatures, but regardless of doping, as the temperature decreases, the effective hybridization strength is significantly suppressed. This is due to the formation of a pseudo-gap structure in the cavity electronic density of states. As the pseudo-gap structure arises, the bath electron density of states at the Fermi level  $\rho$  decreases. This reduces the coupling constant  $J_K\rho$  and the effective lattice Kondo coupling  $J^{\text{latt}}$  which determines the coherence scale

$$T^* = \sqrt{2J^{\text{latt}}\rho} \exp\left[-\frac{1}{2J^{\text{latt}}\rho}\right], \quad (5)$$

becomes smaller as a result.

In conclusion, we have studied the temperature scales of the doped Anderson lattice model using single-site dynamical mean field theory. The local Kondo temperature  $T_K$  defined by the Kondo exchange coupling  $J_K$  governs the high-temperature regime, but a new scale  $T^*$ , defined by a modified Kondo lattice exchange coupling  $J^{\text{latt.}}$  gov-

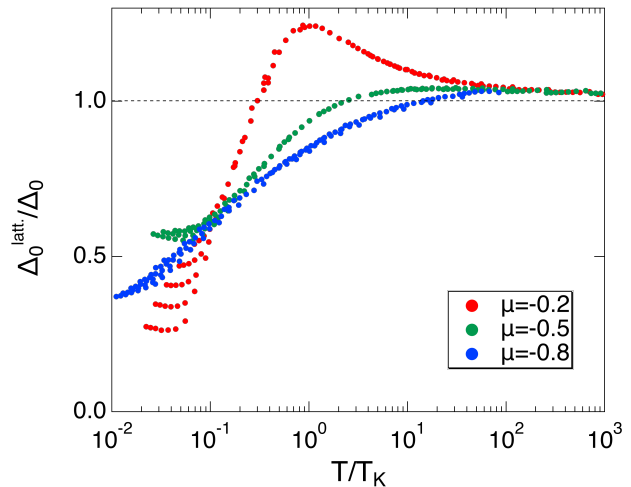


FIG. 5. Ratio between effective hybridization strength of the lattice model ( $\Delta_0^{\text{latt.}}$ ) and hybridization strength of the impurity model.

erns the low- $T$  regime.  $T^*$  has clear doping dependency, and it approaches to zero as  $n_c$  goes to zero, but tends to the single-ion  $T_K$  as  $n_c$  approaches half filling. Various physical observables such as spectral function and transport properties are scaled by  $T_K$  at high- $T$  regime, and  $T^*$  at low- $T$  regime.

We have also confirmed that most observables show a significant change at  $T^*$ , which is always significantly smaller than  $T_K$ . The DMFT self consistency determines the suppression and magnitude of  $T^*$ .

This research was supported by Basic Science Research Program through the National Research Foundation of Korea(NRF) funded by the Ministry of Education (2017R1D1A1B03032069), and by DOE Basic energy sciences grant DE-FG02-99ER45790 (PC).

<sup>1</sup> W. J. De Haas, J. De Boer, and G. J. van den Berg, *Physica* **1**, 1115 (1934).

<sup>2</sup> J. Kondo, *Progress of Theoretical Physics* **32**, 37 (1964).

<sup>3</sup> P. W. Anderson, *Journal of Physics C: Solid State Physics* **3**, 2436 (1970).

<sup>4</sup> K. G. Wilson, *Reviews of Modern Physics* **47**, 773 (1975).

<sup>5</sup> K. Wilson, *Physics Reports* **12**, 75 (1974).

<sup>6</sup> K. G. Wilson, *Physical Review B* **4**, 3174 (1971).

<sup>7</sup> P. Nozières, *Journal of Low Temperature Physics* **17**, 31 (1974).

- <sup>8</sup> N. Read and D. M. Newns, *Journal of Physics C: Solid State Physics* **16**, L1055 (1983).
- <sup>9</sup> P. Coleman, *Physical Review B* **35**, 5072 (1987).
- <sup>10</sup> T. Kasuya, *Progress of Theoretical Physics* **16**, 45 (1956).
- <sup>11</sup> S. Doniach, *Physica B+C* **91**, 231 (1977).
- <sup>12</sup> M. A. Ruderman and C. Kittel, *Physical Review* **96**, 99 (1954).
- <sup>13</sup> K. Yosida, *Physical Review* **106**, 893 (1957).
- <sup>14</sup> R. Settai, T. Takeuchi, and Y. Ōnuki, *Journal of the Physical Society of Japan* **76**, 051003 (2007).
- <sup>15</sup> A. C. Hewson, *The Kondo Problem to Heavy Fermions* (Cambridge University Press, 1997).
- <sup>16</sup> M. W. McElfresh, M. B. Maple, J. O. Willis, Z. Fisk, J. L. Smith, and J. D. Thompson, *Physical Review B* **42**, 6062 (1990).
- <sup>17</sup> J. D. Thompson and Z. Fisk, *Physical Review B* **31**, 389 (1985).
- <sup>18</sup> G. R. Stewart, *Reviews of Modern Physics* **56**, 755 (1984).
- <sup>19</sup> S. Burdin and V. Zlatić, *Physical Review B* **79**, 115139 (2009).
- <sup>20</sup> D. Tanasković, K. Haule, G. Kotliar, and V. Dobrosavljević, *Physical Review B* **84**, 115105 (2011).
- <sup>21</sup> Q. Y. Chen, D. F. Xu, X. H. Niu, J. Jiang, R. Peng, H. C. Xu, C. H. P. Wen, Z. F. Ding, K. Huang, L. Shu, et al., *Physical Review B* **96**, 045107 (2017).
- <sup>22</sup> Kummer, K, Patil, S, Chikina, A, Güttler, M, Höppner, M, Generalov, A, Danzenbächer, S, Seiro, S, Hannaske, A, Krellner, C, et al., *Physical Review X* **5**, 011028 (2015).
- <sup>23</sup> A. Georges, G. Kotliar, W. Krauth, and M. J. Rozenberg, *Reviews of Modern Physics* **68**, 13 (1996).
- <sup>24</sup> A. Georges and G. Kotliar, *Physical Review B* **45**, 6479 (1992).
- <sup>25</sup> D. Vollhardt, *Physica B: Condensed Matter* **169**, 277 (1991).
- <sup>26</sup> W. Metzner and D. Vollhardt, *Physical Review Letters* **62**, 324 (1989).
- <sup>27</sup> P. Werner, A. Comanac, L. de' Medici, M. Troyer, and A. J. Millis, *Physical Review Letters* **97**, 076405 (2006).
- <sup>28</sup> R. K. Bryan, *European Biophysics Journal* **18**, 165 (1990).
- <sup>29</sup> M. Jarrell and J. E. Gubernatis, *Physics Reports* **269**, 133 (1996).
- <sup>30</sup> J. R. Schrieffer and P. A. Wolff, *Physical Review* **149**, 491 (1966).
- <sup>31</sup> See supplementary material.
- <sup>32</sup> S. Jang, J. D. Denlinger, J. W. Allen, V. S. Zapf, M. B. Maple, J. N. Kim, B. G. Jang, and J. H. Shim, arxiv 1704.08247 (2017).
- <sup>33</sup> C. Lacroix, *Solid State Communications* **54**, 991 (1985).